Journal of Inflammation Research

Dovepress
open access to scientific and medical research

Open Access Full Text Article

ORIGINAL RESEARCH

Gclc as a Marker for Injured Distal Nephron in Ischemia-Reperfusion Induced Acute Kidney Injury

Yinzheng Li[1], Shulin Ma[1], Zheng Wang[1], Mengxia Shi[1], Rui Zeng[1–4,*], Ying Yao[1,5,*]

[1]Department of Nephrology, Tongji Hospital, Tongji Medical College, Huazhong University of Science and Technology, Wuhan, 430030, People's Republic of China; [2]Key Laboratory of Organ Transplantation, Ministry of Education, Wuhan, 430030, People's Republic of China; [3]NHC Key Laboratory of Organ Transplantation, Wuhan, 430030, People's Republic of China; [4]Key Laboratory of Organ Transplantation, Chinese Academy of Medical Sciences, Wuhan, 430030, People's Republic of China; [5]Department of Nutrition, Tongji Hospital, Tongji Medical College, Huazhong University of Science and Technology, Wuhan, 430030, People's Republic of China

*These authors contributed equally to this work

Correspondence: Ying Yao; Rui Zeng, Department of Nephrology, Tongji Hospital, Tongji Medical College, Huazhong University of Science and Technology, Wuhan, 430030, People's Republic of China, Tel +86 13720379867; +86 15002726366, Email yaoyingkk@126.com; zengrui@tjh.tjmu.edu.cn

Purpose: The distal nephron of kidney plays a pivotal role in advancing acute kidney injury (AKI). Understanding the role of distal nephrons in AKI and identifying markers of injured distal nephrons are critical to comprehending the mechanism of renal injury and identifying novel therapeutic targets.

Methods: We analyzed single-cell RNA sequencing (scRNA-seq) data from mice with AKI induced by ischemia-reperfusion (IR), unilateral ureteral obstruction (UUO), cisplatin (CP), sodium oxalate (SO) and lipopolysaccharide (LPS). Additionally, we analyzed renal transcriptomics samples for AKI. Subsequently, we validated the effectiveness of targeting the biomarker *Gclc* in vitro and in vivo through metabolomics and immunofluorescence.

Results: The LOH-Inj and DCT-Inj subtypes were identified through scRNA-seq. Compared to normal distal nephrons, the injured distal nephrons exhibited higher levels of ferroptosis, pro-inflammation, and fibrosis. The expression of ferroptosis-related gene *Gclc* were high in various AKI models. Furthermore, *Gclc* was exclusively expressed in the distal nephron and upregulated in the injury subtype. To confirm our findings, we suppressed GCLC expression in the kidneys, resulting to aggravated IR-induced AKI. Inhibition of *Gclc* promoted damage to primarily renal tubular epithelial cells by promoting inflammatory infiltration, inhibiting glutathione metabolism and exacerbating oxidative stress.

Conclusion: Our research findings suggest that *Gclc* is a potential marker for injured distal nephron.

Keywords: *Gclc*, distal nephron, acute kidney injury, single-cell sequencing

Introduction

Acute kidney injury (AKI) is a prevalent complication amongst clinical critical patients, with an incidence rate of 15% in hospitalized patients.[1,2] AKI patients face a 2–3 times higher risk of death compared to the average patient,[3] resulting in significant economic and emotional burdens on both patients and society.

As the typical markers of renal function, serum creatinine (CR) and blood urea nitrogen (BUN) are relatively delayed and imprecise to determine the alterations in renal function.[4,5] Furthermore, CR lacks the sensitivity and specificity to differentiate between parenchymal and functional renal injury.[6] Consequently, there is an urgent need for new biomarkers for AKI. In fact, novel biomarkers have become a research hotspot in recent years to improve early detection and treatment of renal injury. However, trustworthy methods for reversing renal damage are still elusive.[7] Therefore, it is crucial to explore renal injury markers in AKI for preventing and delaying the advancement of kidney disease.

In recent years, considerable advancements have been made in characterizing AKI and fibrosis through the utilization of single-cell sequencing (scRNA-seq) technology.[8,9] Research has demonstrated that energy impairment in the highly metabolically active segments of the kidney, specifically the thick ascending limb (TAL) and proximal tubule (PT), is one

Received: 23 November 2023
Accepted: 18 January 2024
Published: 31 January 2024

of the mechanisms of renal injury, which subsequently results in the transition of renal tubular epithelial cells from transient hypoxia to renal failure.[10] Therefore, this study focused on distal tubular epithelial cells.

GCLC, which is known as the glutamate cysteine ligase catalytic subunit, is an antioxidant enzyme that acts as the rate-limiting step in glutathione (GSH) biosynthesis.[11] It has been utilized by various studies as an indicator of reactive oxygen species (ROS) levels in cells or organisms.[12,13] In addition, studies have linked GCLC to ferroptosis, which is characterized by lipid peroxidation and is dependent on both iron and ROS.[14] It has been suggested that *Gclc* is a ferroptosis-related gene and a new prognostic biomarker for patients with lung adenocarcinoma.[15] Overexpression of GCLC inhibited ferroptosis induced by Influenza A virus in human nasal epithelial progenitor cells, consequently suppressing the inflammatory response of nasal mucosal epithelium.[16]

Limited research has been conducted on *Gclc* in kidney, but studies on other organs suggest that *Gclc* knockout contribute to disease progression. Specifically, mice with *Gclc* deletion in pancreatic endocrine progenitor cells exhibited a progressive diabetic phenotype,[17] while lack of *Gclc* in the central nervous system of mice resulted in mitochondrial damage and neurodegeneration.[18] Bone marrow mesenchymal stem cells that overexpress GCLC was found to alleviate acute lung injury through anti-apoptotic effects.[19]

In this study, the transcriptional characteristics of distal renal tubules in various AKI models were analyzed using scRNA-seq data from Zhimin Chen et al.[20] The marker *Gclc* of the distal renal tubule was identified through scRNA-seq and renal transcriptomics data. Furthermore, the role of *Gclc* in acute kidney injury was explored by targeting *Gclc*. This research laid a solid foundation for discovering therapeutic targets for AKI.

Material and Methods

Ethics Statement

The Human Ethics Approval has been approved by the Medical Ethics Committee of Tongji Hospital, Tongji Medical College, Huazhong University of Science and Technology (TJ-IRB20230446). Data on patients with renal transplant dysfunction were obtained from pathological specimens of kidney punctures of hospitalized patients at Tongji Hospital, Tongji Medical College, Huazhong University of Science and Technology.

The animal ethics approval has been approved by the Science Ethics Committee of Huazhong Agricultural University (HZAUMO-2023-0022). This study was conducted in accordance with the tenets of the Declaration of Helsinki and all procedures involving animal testing were conducted in accordance with the Regulations on the Administration of Experimental Animals in China (1988, amended in 2017).

Bioinformatics Analysis

The single-cell RNA sequencing (scRNA-seq) data used in this article was from the GSE197266 dataset on the GEO platform. The IR H5 transcriptome data was obtained from GSE185383, the UUO H3 transcriptomics data was from GSE174289, and CP H48 and LPS H48 data were derived from GSE240304.

Seurat R package version 4.2.0 was used for further analysis. We excluded cells with gene counts below 400 and above 4000, as well as high mitochondrial transcription levels exceeding 30%, to eliminate low-quality cells. In total, 81383 cells were retained for subsequent analysis. The initial analysis identified 2000 highly variable genes for SCT integration. Clustering results were visualized using Umap and Tsne analysis. Pathway enrichment analysis was performed using ClusterProfiler package. Cell gene expression was analyzed and visualized using Plot1cell package. For comprehensive intercellular communication analysis, Cellchat package was utilized. Finally, we utilized the Scenic package to perform analysis of transcription factors.

Mice Model

C57BL/6 male mice weighing 18–25g were obtained from Beijing Huafu Kang Biotechnology Co., Ltd. All animals were housed in a standard specific pathogen-free (SPF) environment and received complimentary food and water.

The bilateral renal ischemia-reperfusion (IR) injury model: Anesthetize the mice and use a temperature regulator (from FHC in the US) to maintain their body temperature at 36.8–37.2°C. Then, remove hair from the back of the mice, disinfect

with iodine, cut open the skin and muscle layer, detach the bilateral kidneys, and clamp the renal blood vessels of the mice with arterial clamps (from Roboz Surgical Instrument Co, Germany) for 30 minutes. Finally, release the arterial clamp and suture the incision. Collect kidney samples on days 1, 7, and 14 post-reperfusion for further experimentation.

The unilateral ureteral obstruction (UUO) injury model starts with anesthesia, followed by temperature adjustment of the mice to 36.8–37.2 °C using a temperature regulator (from FHC in the United States). The next steps include removing hair from the back of the mice, disinfecting with iodine, cutting open the skin and muscle layer from the back, separating the unilateral kidneys, using tweezers to puncture the kidneys from the lower pole, and pulling the silk thread back from the opposite side to ligate the ureter. Collect kidney samples for further experiments at 1 day, 7 days, and 14 days post-ligation.

The procedure for the 5/6 nephrectomy (5/6 Nx) injury model involves anesthetizing the mice, using the temperature regulator (from FHC in the US) to adjust their temperature to 36.8–37.2 °C, and then removing hair from the back of the mice, disinfecting with iodine, cutting open the skin and muscle layer from the back to separate their kidneys. To preserve the adrenal gland, separate it from the kidneys without damaging blood vessel formation. Afterwards, remove both poles of the left kidney and then remove the right kidney. Collect kidney samples for further experiments 14 days after nephrectomy.

The Folic acid (FA) injury model consists of the following procedures: intraperitoneal injection of FA (250mg/kg), and collection of kidney samples for further experiments one day later.

Histopathology

The kidney was fixed in polyformaldehyde, dehydrated, and embedded in paraffin. The sections underwent staining by Periodic Acid Schiff (PAS) and Sirius Red (SR). Two renal pathologists, working in a blinded manner, assessed the staining in ten randomly chosen fields.

The steps of PAS were as follows: the kidney slices were dewaxed and hydrated, soaked in periodic acid for 20 minutes, stained using Schiff reagent, and the staining was terminated when the kidneys turned red. Using hematoxylin to stain the nuclei and then sealing the slices with neutral gum. Evaluation of renal tubular injury based on the extent of renal tubular injury: 0, 0%; 1, <=10%; 2, 11–25%; 3, 26–45%; 4, 46–75%; 5, >76%. Renal tubular injury includes cell necrosis, tubular swelling, tubular dilation, cast formation and brush border loss.

The SR steps are as follows: after dewaxing and hydration of kidney slices, soak them in Sirius Red staining solution for 40 minutes. Subsequently, soak them in anhydrous ethanol for 5 seconds, and then seal them with neutral gum. We determine the degree of renal fibrosis based on the area of stained deep red interstitial collagen fibers.

Culture of Primary Renal Tubular Epithelial Cells

Under sterile conditions, the mice kidneys were cut into small pieces and digested with 0.2% collagenase IV for one hour to obtain a single-cell suspension. The red blood cells were lysed. The resulting precipitate was then resuspended and transferred to a Falcon bacterial culture dish (351029, Corning). It was left to stand for one hour. Interstitial cells and other miscellaneous cells settled at the bottom of the dish. Finally, transfer the supernatant to a new cell culture dish (353003, Corning) containing DMEM/F12 medium supplemented with primary renal tubular epithelial cell growth factors for cultivation and subsequent passage after 72 hours.

Dihydroethidium Staining

Dihydroethidium (DHE) was acquired from Beyotime Biotech based in Shanghai, China. Primary renal tubular epithelial cells in the culture plate were incubated with 2 μM DHE in dark at 37 °C for 30 minutes. Then, wash the cells with new culture medium for three times and observe them under a fluorescence microscope.

Gclc siRNA Transfection

In vivo, C57 mice were subcapsularly injected with 20nmol/20g of *Gclc* siRNA or NC siRNA (RiboBio, China) dissolved in sterile PBS. Three days later, the mice were subjected to IR. One day after the induction of IR, the mice were euthanized, and plasma and kidney samples were collected for experimental analysis.

In vitro, primary renal tubular epithelial cells were cultured until they reached 60% confluence. Dissolve the powdered siRNA at a final concentration of 20 μM by adding RNase-sterile PBS to the *Gclc* siRNA or NC siRNA

(RiboBio, China) packaging tube. Then, siRNA and RNA iMAX reagent (Invitrogen, USA) were added in a 1:1 ratio to 1.5 mL RNase Free EP tubes containing Opti-MEM solution (Gibco, USA). For every 200 μL Opti-MEM, 5 μL of *Gclc* siRNA was added, mixed well by blowing and suction, and left to stand for 10 minutes. The mixed liquid was then added to DMEM/F12 culture medium to transfect cells. After 8 hours, replace it with complete medium. On the third day after transfection, cells were harvested for further experiments and analysis.

Oxygen Glucose Deprivation/Reoxygenation (OGD/R) Model

Cultivate primary renal tubular epithelial cells to a fusion degree of 80–90%, and replace the cell culture medium with D-Glucose free medium (11,966, Gibco, USA). After placing the cells in a 1% hypoxia incubator for 6 hours, replace the medium with normal DMEM/F12 medium and incubate them conventionally for 3 hours of reoxygenation.

Immunofluorescence and Immunohistochemistry Staining

The steps for immunofluorescence staining are as follows: After dewaxing and hydrating the paraffin slides, heat repair was performed using citrate or EDTA. Then, the slides were incubated with serum to block non-specific antigens. The primary antibody was incubated at 4°C overnight, followed by incubation with the second antibody at 37°C for 1 hour. DAPI staining was performed for 10 minutes, and the sample was sealed with glycerol.

The steps for immunohistochemistry staining are as follows: After dewaxing and hydrating the paraffin slides, heat repair was performed using citrate or EDTA. Block the endogenous catalase with 3% H_2O_2. Then, the slides were incubated with serum to block non-specific antigens. The primary antibody was incubated at 4°C overnight, followed by incubation with the second antibody at 37°C for 1 hour. Develop color with DAB staining solution, and stain nucleus with hematoxylin.

Serum SOD and MDA Detection

The SOD concentration was measured with SOD (G4306) kits from Servicebio (China) in accordance with the instructions provided by the manufacturer of the reagent. The MDA (G4300) concentration was measured with MDA kits from Servicebio (China) in accordance with the instructions provided by the manufacturer of the reagent.

Untargeted Metabolomics Analysis Technology

Untargeted metabolomics analysis (LC-MS/MS) was conducted by Novogene Co., Ltd from China. This project utilized LC-MS technology for non-targeted metabolomics research. The experimental process involved sample metabolite extraction, LC-MS/MS detection, and qualitative and quantitative analysis of metabolites. The original files obtained from mass spectrometry detection were imported into Compound Discoverer 3.1 software, spectrum processing and database searching were performed, qualitative and quantitative results of metabolites were obtained, and then quality control of the data was performed to ensure the accuracy and reliability of the results. Multivariate statistical analysis, including qualitative and quantitative analysis, partial least squares discriminant analysis (PLSDA), and metabolite correlation analysis, were conducted to reveal changes in metabolites under different cell treatment conditions.

Quantitative Real Time-PCR

Renal RNA was extracted using Trizol reagent (Invitrogen, USA), followed by reverse transcription into single-stranded cDNA using reverse transcription reagent (Vazyme, China). Quantitative PCR detection was then performed using SYBR Mix (Vazyme, China) on the Step One real-time PCR system (ABI, USA). Relative gene expression was calculated using $2^{-\Delta\Delta CT}$ with *Gapdh* as the endogenous control gene. The primer sequences used are listed in Table 1.

Renal Function

The serum creatinine concentration was measured with the QuantiChrom™ Creatinine Assay Kit (BioAssay Systems, USA) in accordance with the instructions provided by the manufacturer of the reagent. The serum blood urea nitrogen (BUN) concentration was measured with the QuantiChrom™ Urea Assay Kit (BioAssay Systems, USA) in accordance with the instructions provided by the manufacturer of the reagent.

Table 1 List and Sequence for Primers Used for qRT-PCR

Gene	Forward(5'to3')	Reverse(5'to3')
Gapdh	TGACCTCAACTACATGGTCTACA	CTTCCCATTCTCGGCCTTG
Gclc	GGGGTGACGAGGTGGAGTA	GTTGGGGTTTGTCCTCTCCC
Ccl2	TTAAAAACCTGGATCGGAACCAA	GCATTAGCTTCAGATTTACGGGT
Il1b	GCAACTGTTCCTGAACTCAACT	ATCTTTTGGGGTCCGTCAACT
Tnf	CCCTCACACTCAGATCATCTTCT	GCTACGACGTGGGCTACAG
Nox2	TGTGGTTGGGGCTGAATGTC	CTGAGAAAGGAGAGCAGATTTCG
Sod1	AACCAGTTGTGTTGTCAGGAC	CCACCATGTTTCTTAGAGTGAGG
Acsl4	CTCACCATTATATTGCTGCCTGT	TCTCTTTGCCATAGCGTTTTTCT
Lpcat2	GACGGGGACATGGGAGAGA	GTAAAACAGAGCCAACGGGTAG

Statistical Analysis

The data were analyzed using GraphPad Prism software version 6.0. The normal distribution data was represented by the mean ± SEM.* $P < 0.05$, * * $P < 0.01$, * * * $P < 0.001$.

Results

Injured Distal Nephron Exhibited Higher Activity Than the Normal Distal Nephron

We analyzed the transcriptional characterization of kidneys in AKI models induced by cisplatin (CP), folic acid (FA), ischemia-reperfusion (IR), sodium oxalate (SO) and unilateral ureteral obstruction (UUO) using scRNA-seq data obtained from GSE197266. We defined 14 cell types, including T lymphocytes (T cell), B lymphocytes (B cell), macrophages (Macro), endothelial cells (EC), neutrophils (Neutro), dendritic cells (DC), natural killer cells (NK), proximal renal tubular cells (PT), loop of Henle cells (LOH), distal convoluted tubule cells (DCT), intercalated cells of collecting duct cells (CDIC), principal cells of collecting duct cells (CDPC), podocytes (Podo) and myoblasts (Myo) (Figure 1A–B). Subsequently, we isolated LOH, DCT, CDIC and CDPC as distal nephron for further analysis and identified two injury subtypes as DCT-Inj and LOH-Inj (Figure 1C). LOH-Inj was co-labeled with the LOH markers *Umod* and *Slc12a1*, as well as injury markers *Havcr1* and *Krt20*. DCT-Inj was co-labeled with DCT markers *Slc12a3* and *Trpm6*, along with injury markers *Il1f6* and *Nrp1* (Figure 1D). The proportion of injury distal renal tubules was basically higher in CP, FA, IR, SO and UUO models when compared to normal cells (Figure 1E).

Meanwhile, we analyzed the crosstalk between different cells in AKI with Cellchat package. DCT-Inj and LOH-Inj communicated more closely with other cells as senders or receivers compared to DCT and LOH (Figure 1F). In AKI induced by IR (Supplementary Figure S1A–S1B) and UUO (Supplementary Figure S1C–S1D), our findings indicated that injured distal nephron associated with activated SPP1 pathway in both IR and UUO models. In IR, the inflammatory pathway was more pronounced whereas in UUO, the fibrotic pathway was more prominent.

This suggested that in AKI, the injured distal nephron exhibited higher activity than the normal distal nephron.

The Levels of Ferroptosis Increased in DCT-Inj and LOH-Inj When Compared to Normal DCT and LOH

After analyzing the Kyoto Encyclopedia of Genes and Genomes (KEGG) pathway in DCT-Inj and LOH-Inj, we observed elevated levels of ferroptosis, ECM-receptor interaction, and focal adhesion when compared to normal DCT and LOH. Meanwhile, we found that the levels of oxidative phosphorylation (OXPHOS) and citrate cycle (TCA) decreased (Figure 2A–B).

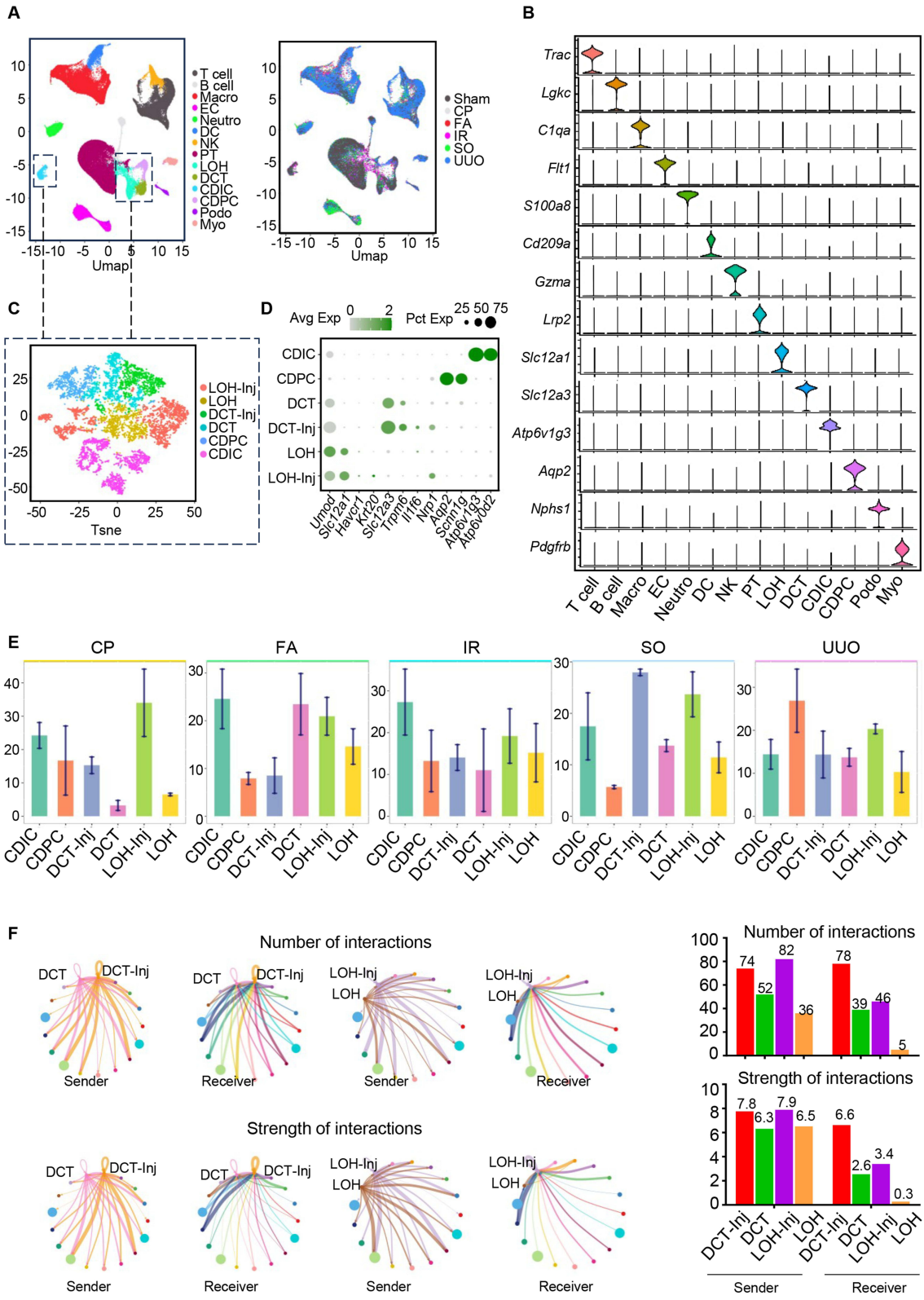

Figure 1 An Atlas of Single-Cell Sequencing of Kidney in AKI in Mice. (A) Umap plot of scRNA-seq from mice kidneys of AKI induced by cisplatin (CP), folic acid (FA), ischemia-reperfusion (IR), sodium oxalate (SO) and unilateral ureteral obstruction (UUO). (B) Vlnplot of marker genes in different cell subtypes. (C) Tsne plot of subtypes of distal nephron. (D) Dotplot of injury subtypes in distal nephrons. (E) Proportion of distal renal tubular cells in CP, FA, IR, SO and UUO models. (F) DCT, DCT-Inj, LOH and LOH-Inj served as senders and receivers to communicate with other cells, respectively.

Abbreviations: T cell, T lymphocyte; B cell, B lymphocyte; Macro, macrophage; EC, endothelial cell; Neutro, neutrophil; DC, dendritic cell; NK, natural killer cell; PT, proximal renal tubular cell; LOH, loop of Henle cell; DCT, distal convoluted cell; CDIC, intercalated cells of collecting duct; CDPC, principal cells of collecting duct; Podo, Podocyte; Myo, Myoblast.

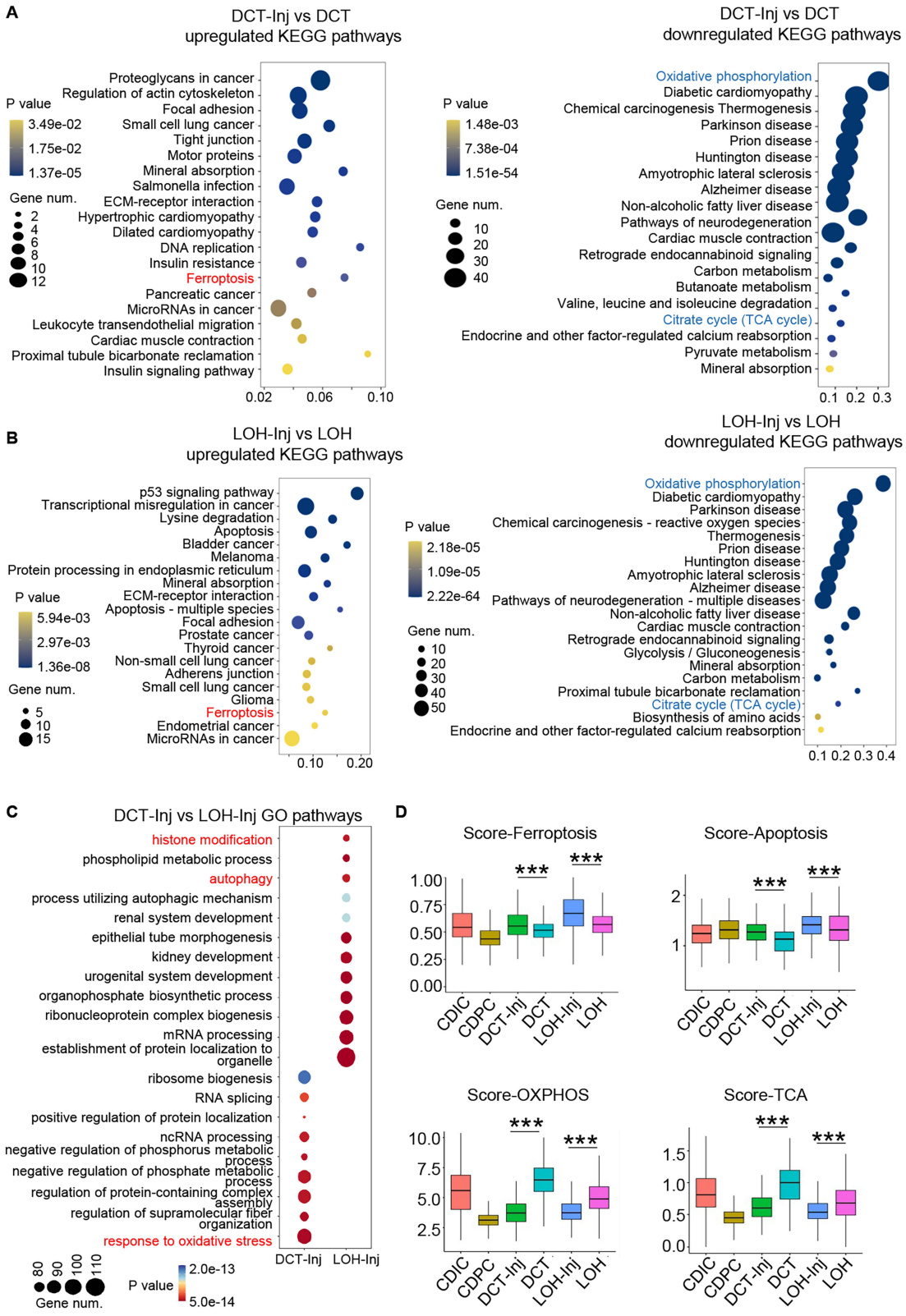

Figure 2 The levels of ferroptosis increased in DCT-Inj and LOH-Inj. (**A**) DCT-Inj upregulated and downregulated KEGG pathways compared to DCT. (**B**) LOH-Inj upregulated and downregulated KEGG pathways compared to LOH. (**C**) GO pathways enriched in DCT-inj compared to LOH-inj. (**D**) Ferroptosis, apoptosis, oxidative phosphorylation (OXPHOS) and tricarboxylic acid cycle (TCA) scores of distal renal tubule cells. The pathways in red are upregulated KEGG pathways of interest, and pathways in blue are downregulated KEGG pathways of focus. ***$P < 0.001$ as determined by one-way ANOVA. Data represent mean ± SEM.

The Gene Ontology (GO) analysis between DCT-Inj and LOH-Inj revealed that DCT-Inj was more responsive to oxidative stress, whereas LOH-Inj was more involved in histone modification and autophagy(Figure 2C). The ferroptosis, apoptosis, OXPHOS and TCA levels in different status distal nephron were scored (Figure 2D). Injured distal nephrons exhibited higher levels of ferroptosis and apoptosis and lower levels of OXPHOS and TCA compared to normal distal nephrons.

This indicated that DCT-Inj and LOH-Inj shared similarities while also presenting differences. Among these, an increase in ferroptosis levels was one commonality between DCT-Inj and LOH-Inj.

Gclc Was an Injury Marker for Distal Tubular Cells

Analysis of genesets related to ferroptosis in renal bulk-RNA sequencing from AKI models with IR H5, UUO H3, CP H48, and LPS H48 demonstrated a significant increase in *Gclc* expression (Figure 3A).

Upon analyzing the expression of *Gclc, Acsl4*, and *Spp1* in renal cells with scRNA-seq, we discovered that *Gclc* was specifically expressed in distal nephron, while ferroptosis marker *Acsl4* was expressed in both distal nephron and podocytes. Meanwhile, *Spp1* displayed wider expression and was detected in most cells (Figure 3B). Further analysis indicated that *Gclc* expression was higher in DCT-Inj and LOH-Inj compared to normal DCT and LOH (Figure 3C).

The characteristics of transcription factors in DCT-Inj and LOH-Inj were analyzed using the Scenic package. The results indicated that the highly active transcription factor ZMIZ1 in DCT-inj and the highly active transcription factor BHLHE40 in LOH-inj promoted the transcription of *Gclc* (Supplementary Figure S2A–S2B). The representative transcription factors, *Zmiz1* and *Ppargc1a*, exhibited opposing transcriptional activity sites between DCT-Inj and DCT (Supplementary Figure S2C). Similarly, *Bhlhe40* and *Hnf4a* exhibited opposite sites of transcriptional activity between LOH-Inj and LOH (Supplementary Figure S2D). Meanwhile, we utilized the JASPAR database and the Scenic R package to predict the motifs of the transcription factors ZMIZ1 and BHLHE40, as well as their binding sites to the target gene *Gclc* (Supplementary Figure S2E–S2F).

Due to the significant increase in ferroptosis levels in IR and the subsequent increase observed in UUO, as shown in the study by Zhimin Chen et al,[20] we established mouse models for both IR and UUO at 1 day, 7 days, and 14 days. In IR, we noted a gradual worsening of renal injury and fibrosis over time, along with a significant increase for ACSL4 as early as IR D1 (Supplementary Figure S3A). In UUO, we observed a gradual worsening of renal injury and fibrosis over time, with the ferroptosis marker ACSL4 gradually increases over time (Supplementary Figure S3B). Immunofluorescence staining with kidney injury marker KIM-1 confirmed extensive damage to renal tubules following IR and UUO, indicating successful modeling (Supplementary Figure S3C). Due to the significant increase in ferroptosis levels during IR D1, we decided to use the IR D1 model for subsequent intervention experiments.

The expression of GCLC was confirmed in Sham, IR D1, IR D7, IR D14, UUO D1, FA D1, and 5/6 nephrectomy (5/6 Nx) D14, by immunofluorescence staining. Notably, GCLC was upregulated in IR, UUO, FA and 5/6 Nx models (Figure 3D). Additionally, GCLC was upregulated in renal tubular cells in transplant renal insufficiency patients compare to minimal change disease patients (Figure 3E). To confirm the expression site of GCLC in the kidney, we co-stained GCLC with markers for the distal convoluted tubule (NCC), loop of Henle (AQP1), collecting duct (DBA), injury distal tubule (LCN2), and proximal tubule (LTL). We found that GCLC was not expressed in the proximal tubule or glomerulus, but in the injury distal tubule. The site marked by white dotted lines represents the glomerulus (Figure 3F).

These results indicated that *Gclc* was upregulated in multiple kidney injury models, and *Gclc* was expressed in injury distal renal tubular epithelial cells.

Targeted *Gclc* Exacerbated IR-Induced AKI

To confirm the effect of *Gclc* in renal injury, *Gclc* expression was suppressed by injecting *Gclc* siRNA into the renal subcapsule before IR. The inhibitory effect was confirmed by immunofluorescence (Figure 4A). Results from PAS, KIM-1 and ACSL4 immunofluorescence, and renal function markers (BUN and CR) demonstrated that the inhibition of *Gclc* exacerbated renal injury even further (Figure 4B–D). The levels of SOD and MDA in mice serum, as well as staining with DHE (capable for detecting reactive oxygen species) in primary renal tubular epithelial cells in oxygen glucose deprivation/reoxygenation (OGD/R), demonstrated that inhibition of *Gclc* intensified oxidative stress (Figure 4D–E), resulting in the progression of kidney

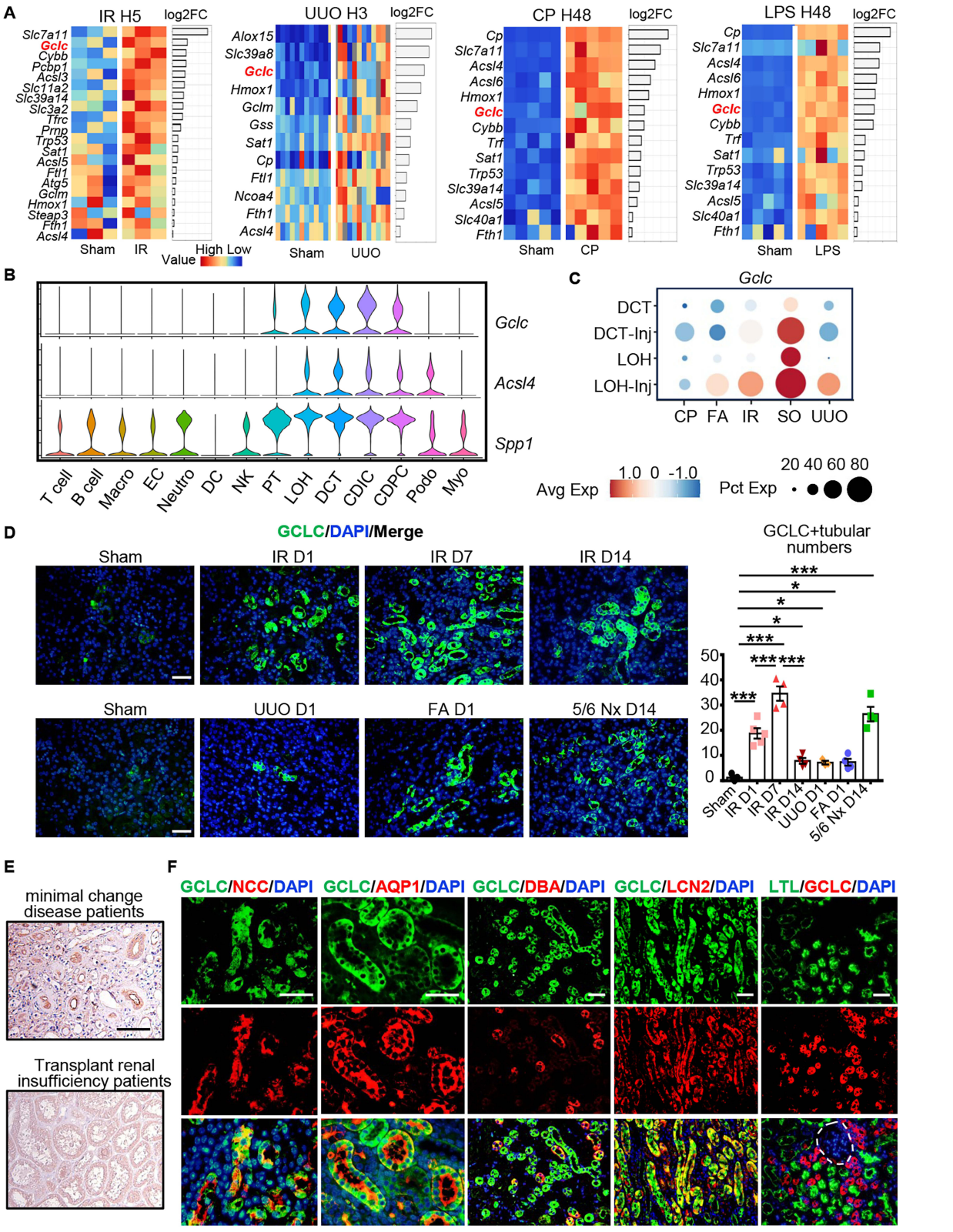

Figure 3 GCLC expression was upregulated in various kidney injury models. (A) Transcriptome heatmaps related to renal ferroptosis at IR H5, UUO H3, CP H48, and LPS H48. (B) Vlnplot of *Gclc*, *Acsl4*, and *Spp1* in different cell subtypes. (C) Dotplot of *Gclc* in different subtypes of distal nephron. (D) Immunofluorescence and scoring of GCLC in IR D1, IR D7, IR D14, UUO D1, FA D1, and 5/6 Nx D14 (n = 4–5 per group). (E) Immunohistochemical staining of GCLC in minimal change disease patients and transplant renal insufficiency patients. (F) Immunofluorescence co-staining of GCLC with distal convoluted tubule marker NCC, loop of Henle marker AQP1, collecting duct marker DBA, injury distal tubule marker LCN2, and proximal tubule marker LTL, respectively. Site marked by white dotted lines was glomeruli. *P < 0.05, ***P < 0.001 as determined by one-way ANOVA. Scale bar, 20 μm. Data represent mean ± SEM.

https://doi.org/10.2147/JIR.S451402 DovePress

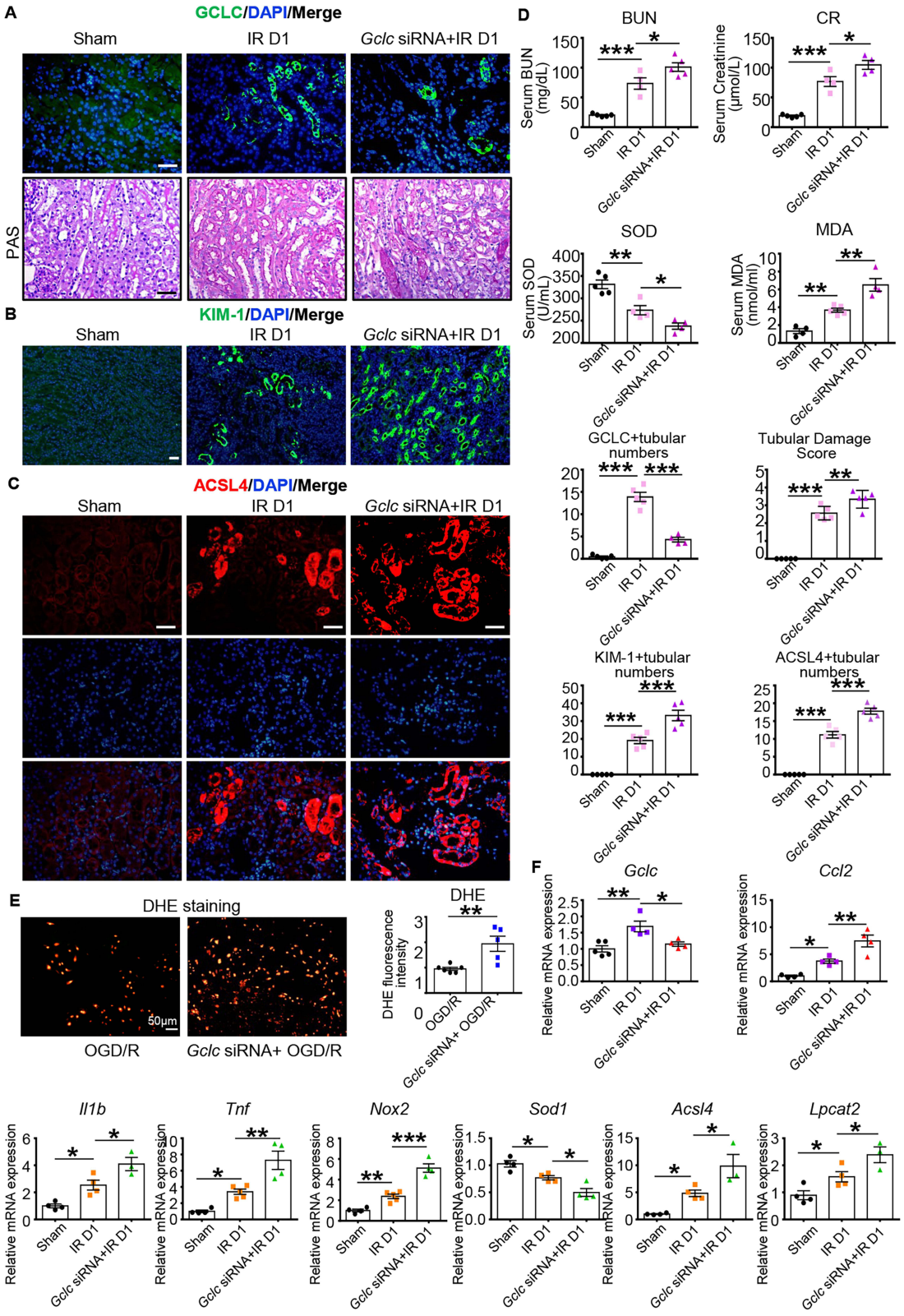

Figure 4 Targeted *Gclc* exacerbated IR induced AKI. (**A**) Immunofluorescence staining of GCLC, as well as PAS staining, and their corresponding scoring in the Sham, IR D1, and *Gclc* siRNA+IR D1 groups (n = 4–5 per group). Scale bar, 20 μm. (**B**) Immunofluorescence staining and scoring of KIM-1 in Sham, IR D1, and *Gclc* siRNA+IR D1 groups (n = 4–5 per group). Scale bar, 20 μm. (**C**) Immunofluorescence staining and scoring of ACSL4 in Sham, IR D1, and *Gclc* siRNA+IR D1 groups (n = 5 per group). Scale bar, 20 μm. (**D**) Detection of BUN and CR, as well as serum SOD and MDA in Sham, IR D1, and *Gclc* siRNA+IR D1 groups (n = 4–5 per group). (**E**) Dihydroethidium (DHE) staining and scoring of oxygen glucose deprivation/reoxygenation (OGD/R) and *Gclc* siRNA+ OGD/R groups in primary renal tubular epithelial cells (n = 5–6 per group). Scale bar, 50 μm. (**F**) The levels of *Gclc*, inflammation-related factors (*Ccl2*, *Il1b*, and *Tnf*), oxidative stress-related indicators (*Nox2* and *Sod1*), and ferroptosis-related indicators (*Acsl4* and *Lpcat2*) were measured using RT-qPCR. *P < 0.05, **P < 0.01, ***P < 0.001 as determined by one-way ANOVA. Data represent mean ± SEM.

disease. Using RT-qPCR, we confirmed that silencing *Gclc* resulted in a decrease in its expression level. Furthermore, the levels of inflammation-related factors (*Ccl2, Il1b*, and *Tnf*), oxidative stress-related indicators (*Nox2* and *Sod1*), and ferroptosis-related indicators (*Acsl4* and *Lpcat2*) suggested an increase in renal inflammation, oxidative stress, and ferroptosis(Figure 4F).

At the same time, we conducted metabolomics analysis on primary renal tubular epithelial cells after OGD/R, and PLSDA plot showed significant differences between the OGD/R and *Gclc* siRNA + OGD/R groups (Figure 5A). After *Gclc* inhibition, reduced glutathione, L (-)-carnitine, and the glutathione precursor Cys-Gly decreased, while noradrenaline, prostaglandin, histamine, LPS and S-(Methyl)glutathione significantly increased (Figure 5B–C). Of note, S-(Methyl) glutathione suppressed the activity of the detoxification enzyme glyoxalase 1, leading to cytotoxicity and tissue damage. Correlation analysis revealed that reduced glutathione, L (-) - carnitine, and Cys-Gly were negatively correlated with noradrenaline, prostaglandin, histamine, S-(Methyl)glutathione and LPS (Figure 5D).

Therefore, we concluded that inhibition of *Gclc* exacerbated renal injury. Inhibition of *Gclc* promoted damage to renal tubular epithelial cells by inhibiting glutathione metabolism and exacerbating oxidative stress.

Discussion

Renal tubular injury plays a crucial role in the development of renal disease. Currently, there has been extensive research on proximal renal tubular injury,[21–23] whereas studies on markers of distal renal tubular injury and patterns of injury have been limited due to the complexity of distal nephron origins and the diversity of cellular subpopulations.[24,25] Long-term renal injury has been found to result in increased expression of *Sox4* and *Hox* genes in distal tubular segments.[26] However, the patterns of acute-phase injury in these segments remain poorly understood. Consequently, a thorough evaluation of crucial molecules and intercellular communication linked to distal renal tubular injury in AKI is necessary.

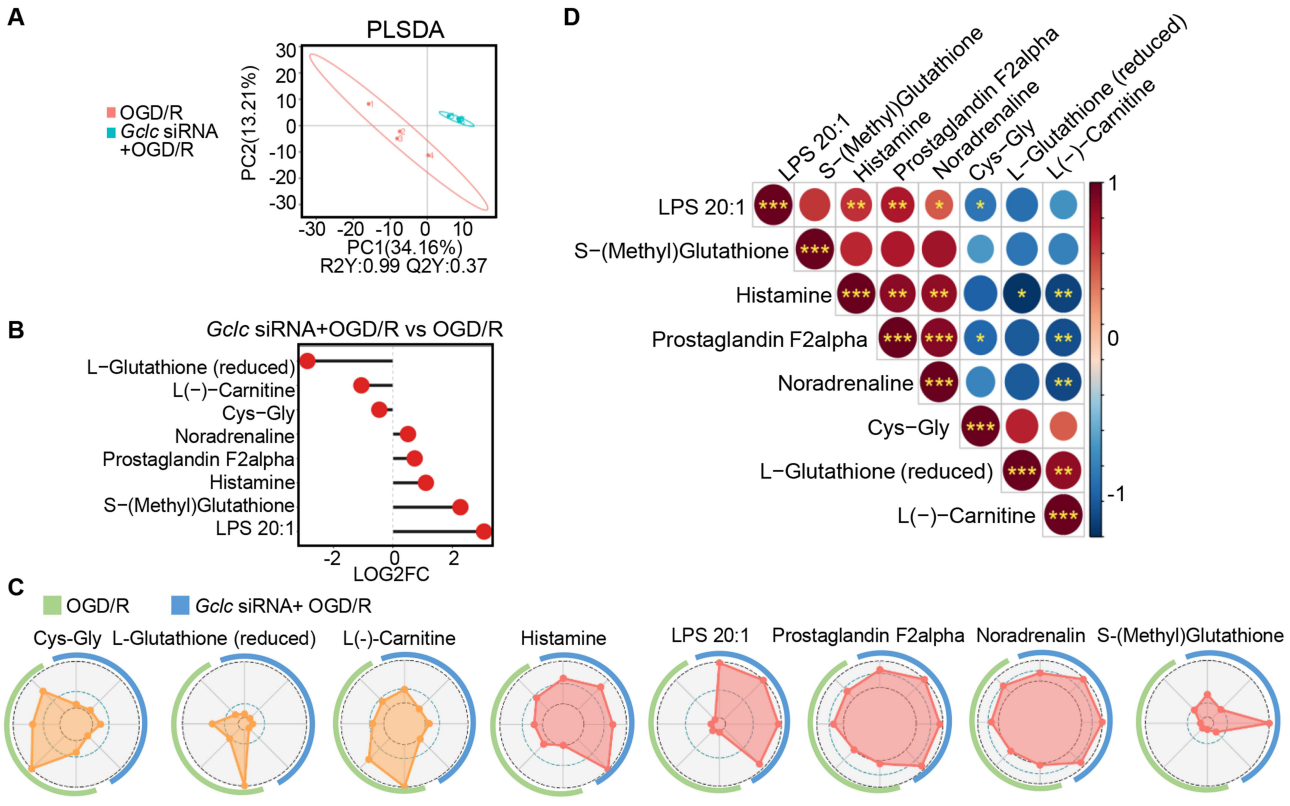

Figure 5 Targeting *Gclc* altered metabolic levels in the kidney. (**A**) PLSDA plots of OGD/R group and *Gclc* siRNA +OGD/R group in metabolomics (n = 4 per group). (**B**) Lollipop plot of representative metabolites in the *Gclc* siRNA+OGD/R group compared to OGD/R group (n = 4 per group). (**C**) Radar plot of representative metabolites in the *Gclc* siRNA+OGD/R group compared to OGD/R group (n = 4 per group). (**D**) Correlation analysis plot of representative metabolites (n = 4 per group). *P < 0.05, **P < 0.01, ***P < 0.001 as determined by one-way ANOVA.

First, through scRNA-seq analysis, we discovered novel subtypes of injured DCT and LOH cells. We observed that both DCT-Inj and LOH-Inj exhibit increased ferroptosis levels when compared to normal distal renal tubular cells. The transcriptomic characteristics associated with renal ferroptosis in AKI caused by IR, UUO, CP, and LPS were analyzed, revealing high *Gclc* expression levels. ScRNA-seq data indicated that *Gclc* expression was exclusive to distal nephron, with significant levels observed in DCT-Inj and LOH-Inj cells. These results suggested that *Gclc* was a potential marker of renal injury in distal tubular cells.

Numerous studies have confirmed that *Gclc* functions as an antioxidant and inhibits ferroptosis.[27–30] Since *Gclc* was significantly upregulated at 5 hours after IR and 3 hours after UUO, we hypothesized that the increase in *Gclc* expression in distal nephron during the early stage of renal injury was a self-help mechanism of tubular cells. The tubular cells likely attempted to resist further damage through anti-oxidative stress. The upregulation of *Gclc* expression was probably earlier than most other markers of kidney injury.

To investigate why GCLC express in injured distal renal tubular epithelial cells, we analyzed transcription factor activities using the Scenic package. We found that ZMIZ1 and BHLHE40 promote gene transcription of *Gclc* in DCT-Inj and LOH-Inj, respectively. We predicted the possible binding sites of ZMIZ1 and BHLH40 as transcription factors to the *Gclc* promoter region. This demonstrated that DCT-Inj and LOH-Inj may promote *Gclc* gene transcription through ZMIZ1 and BHLH40 activation. Studies revealed that ZMIZ1 was closely associated with oxidative stress,[31] while BHLH40 mediated lipid peroxidation, a classical feature of ferroptosis.[32] This suggests that injured renal tubular epithelial cells may activate ZMIZ1 and BHLH40 to promote GCLC expression after renal injury. However, further mechanistic studies are necessary to obtain definitive evidence.

To confirm the protective function of *Gclc* in kidney injury, we inhibited *Gclc* expression by injecting *Gclc* siRNA into the subcapsular space in the kidney. Our findings indicated that inhibiting *Gclc* intensified kidney injury. At the same time, we conducted metabolomics analysis on primary renal tubular epithelial cells after OGD/R. After inhibiting *Gclc*, the levels of reduced glutathione and the glutathione precursor Cys-Gly decreased. Meanwhile, metabolites like LPS and histamine that promote cell damage increased. This suggests that inhibiting *Gclc* worsens the harm to renal tubular cells by inhibiting glutathione metabolism and exacerbating oxidative stress.

When analyzing the communication of DCT-Inj and LOH-Inj with other kidney cells, we found that the secreted phosphoprotein 1 (SPP1) pathway was co-activated in injury distal renal tubular cells in both IR and UUO. In IR, DCT-Inj served as a sender and receiver in SPP1 signaling pathway, while LOH-Inj primarily received SPP1 signals from almost all cells. In UUO, LOH-Inj mainly send signals to CDIC, DCT-Inj, and Podo. Studies have demonstrated that SPP1, a member of the small integrin-binding ligand N-linked glycoprotein (SIBLING) family,[33,34] is involved in the pathogenicity of the renal tubular microenvironment.[35] Ferroptosis was suppressed in astrocytes and neuroblastoma N2a cells by targeting SPP1.[36,37] Our hypothesis suggests that co-activation of SPP1 in IR and UUO models leads to increased levels of ferroptosis.

Except for SPP1, DCT-Inj and LOH-Inj had unique communication modes in both IR and UUO. Specifically, in IR, DCT-Inj send MIF and PDGF signals, and received TNF and TWEAK signals, whereas LOH-Inj send CX3C and PGDF signals, and received TNF and TWEAK signals. In UUO, DCT-Inj received the TGFb signal. This demonstrated that the communication patterns of DCT-Inj and LOH-Inj in IR and UUO are similar but differentiated. Inflammatory pathways were more pronounced in IR and fibrotic pathways in UUO.

Current studies have demonstrated increased *Gclc* expression in kidney injury induced by UUO and IR.[38,39] Moreover, in Atrazine (ATR)-induced kidney injury, there's an upregulation of GCLC.[40] Our research confirms the upregulation of GCLC expression in various injury models and specifically identifies its expression in the injured distal renal tubules. Furthermore, intervening in GCLC exacerbates kidney injury, representing the innovative aspect of our study.

In conclusion, our study highlights the potential of *Gclc* as a therapeutic target for distal renal tubular injury. *Gclc* protects the kidneys by inhibiting inflammation and oxidative stress and promoting glutathione metabolism.

Conclusion

Gclc is a potential marker for injured distal nephron. *Gclc* protects the kidneys by inhibiting inflammation and oxidative stress and promoting glutathione metabolism.

Abbreviations

scRNA-seq, single-cell sequencing; AKI, acute kidney injury; IR, ischemia-reperfusion; UUO, unilateral ureteral obstruction; CP, cisplatin; SO, sodium oxalate; FA, Folic acid; LPS, lipopolysaccharide; CR, serum creatinine; BUN, blood urea nitrogen; TAL, the thick ascending limb; PT, proximal tubular cells; DCT, distal convoluted tubular cells; GSH, glutathione; ROS, reactive oxygen species; 5/6 Nx, 5/6 nephrectomy; PAS, Periodic Acid Schiff; DHE, Dihydroethidium; Macro, macrophages; EC, endothelial cells; Neutro, neutrophils; DC, dendritic cells; NK, natural killer cells; LOH, loop of Henle cells; CDIC, intercalated cells of collecting duct cells; CDPC, principal cells of collecting duct cells; Podo, podocytes; Myo, myoblasts; KEGG, Kyoto Encyclopedia of Genes and Genomes; OXPHOS, oxidative phosphorylation; TCA, citrate cycle; GO, Gene Ontology; OGD/R, oxygen glucose deprivation/reoxygenation.

Acknowledgments

The author extends sincere appreciation to all study participants. This research was financially supported by the National Natural Science Foundation of China (Grants No. 82170701and 81974087). Figures 2A-2C, 3A, 5B-5D, and Supplementary Figure S2A and S2B were performed using the OmicStudio tool on https://www.omicstudio.cn/tool.

Disclosure

The authors declared that they have no conflicts of interest in this work.

References

1. Rossaint J, Zarbock A. Acute kidney injury: definition, diagnosis and epidemiology. *Minerva Urol. Nefrol*. 2016;68(1):49–57.
2. Vijayan A. Tackling AKI: prevention, timing of dialysis and follow-up. *Nat Rev Nephrol*. 2021;17(2):87–88. doi:10.1038/s41581-020-00390-3
3. Coca SG, Singanamala S, Parikh CR. Chronic kidney disease after acute kidney injury: a systematic review and meta-analysis. *Kidney Int*. 2012;81(5):442–448. doi:10.1038/ki.2011.379
4. Joliat GR, Labgaa I, Demartines N, Halkic N. Acute kidney injury after liver surgery: does postoperative urine output correlate with postoperative serum creatinine? *HPB (Oxford)*. 2020;22(1):144–150. doi:10.1016/j.hpb.2019.06.016
5. Finco DR, Duncan JR. Evaluation of blood urea nitrogen and serum creatinine concentrations as indicators of renal dysfunction: a study of 111 cases and a review of related literature. *J. Am. Vet. Med. Assoc*. 1976;168(7):593–601.
6. Moledina DG, Parikh CR. Phenotyping of acute kidney injury: beyond serum creatinine. *Semin. Nephrol*. 2018;38(1):3–11. doi:10.1016/j.semnephrol.2017.09.002
7. Gumbert SD, Kork F, Jackson ML, et al. Perioperative acute kidney injury. *Anesthesiology*. 2020;132(1):180–204. doi:10.1097/ALN.0000000000002968
8. Rudman-Melnick V, Adam M, Potter A, et al. Single-cell profiling of aki in a murine model reveals novel transcriptional signatures, profibrotic phenotype, and epithelial-to-stromal crosstalk. *J. Am. Soc. Nephrol*. 2020;31(12):2793–2814. doi:10.1681/ASN.2020010052
9. Li H, Dixon EE, Wu H, Humphreys BD. Comprehensive single-cell transcriptional profiling defines shared and unique epithelial injury responses during kidney fibrosis. *Cell Metab*. 2022;34(12):1977–1998 e1979. doi:10.1016/j.cmet.2022.09.026
10. Basile DP, Anderson MD, Sutton TA. Pathophysiology of acute kidney injury. *Compr Physiol*. 2012;2:1303–1353. doi:10.1002/cphy.c110041
11. Ran S, Gao X, Ma M, et al. NaAsO(2) decreases GSH synthesis by inhibiting GCLC and induces apoptosis through Hela cell mitochondrial damage, mediating the activation of the NF-kappaB/miR-21 signaling pathway. *Ecotoxicol. Environ. Saf*. 2022;234:113380. doi:10.1016/j.ecoenv.2022.113380
12. You GR, Chang JT, Li Y-L, et al. MYH9 facilitates cell invasion and radioresistance in head and neck cancer via modulation of cellular ROS levels by activating the MAPK-Nrf2-GCLC pathway. *Cells*. 2022;11(18):2855. doi:10.3390/cells11182855
13. Hseu YC, Vudhya Gowrisankar Y, Wang L-W, et al. The in vitro and in vivo depigmenting activity of pterostilbene through induction of autophagy in melanocytes and inhibition of UVA-irradiated alpha-MSH in keratinocytes via Nrf2-mediated antioxidant pathways. *Redox Biol*. 2021;44:102007. doi:10.1016/j.redox.2021.102007
14. Kajarabille N, Latunde-Dada GO. Programmed cell-death by ferroptosis: antioxidants as mitigators. *Int. J. Mol. Sci*. 2019;20(19):4968. doi:10.3390/ijms20194968
15. Luo L, Zhang Z, Weng Y, Zeng J. Ferroptosis-related gene GCLC is a novel prognostic molecular and correlates with immune infiltrates in lung Adenocarcinoma. *Cells*. 2022;11(21):3371. doi:10.3390/cells11213371
16. Liu C, Wu X, Bing X, et al. H1N1 influenza virus infection through NRF2-KEAP1-GCLC pathway induces ferroptosis in nasal mucosal epithelial cells. *Free Radic. Biol. Med*. 2023;204:226–242. doi:10.1016/j.freeradbiomed.2023.05.004
17. Davidson EA. Endocrine pancreas-specific Gclc gene deletion causes a severe diabetes phenotype. *bioRxiv*. 2023. doi:10.1101/2023.06.13.544855
18. Feng W, Rosca M, Fan Y, et al. Gclc deficiency in mouse CNS causes mitochondrial damage and neurodegeneration. *Hum. Mol. Genet*. 2017;26(7):1376–1390. doi:10.1093/hmg/ddx040
19. Zhang Z, Kuang Y, Ma K, et al. Gclc overexpression inhibits apoptosis of bone marrow mesenchymal stem cells through the PI3K/AKT/Foxo1 pathway to alleviate inflammation in acute lung injury. *Int. Immunopharmacol*. 2022;110:109017. doi:10.1016/j.intimp.2022.109017
20. Chen Z, Li Y, Yuan Y, et al. Single-cell sequencing reveals homogeneity and heterogeneity of the cytopathological mechanisms in different etiology-induced AKI. *Cell Death Dis*. 2023;14(5):318. doi:10.1038/s41419-023-05830-z

21. Wu H, Gonzalez Villalobos R, Yao X, et al. Mapping the single-cell transcriptomic response of murine diabetic kidney disease to therapies. *Cell Metab*. 2022;34(7):1064–1078.e6. doi:10.1016/j.cmet.2022.05.010
22. Wu J, Sun Z, Yang S, et al. Kidney single-cell transcriptome profile reveals distinct response of proximal tubule cells to SGLT2i and ARB treatment in diabetic mice. *Mol. Ther*. 2022;30(4):1741–1753. doi:10.1016/j.ymthe.2021.10.013
23. Guo X, Xu L, Velazquez H, et al. Kidney-targeted renalase agonist prevents cisplatin-induced chronic kidney disease by inhibiting regulated necrosis and inflammation. *J. Am. Soc. Nephrol*. 2022;33(2):342–356. doi:10.1681/ASN.2021040439
24. Trepiccione F, Soukaseum C, Iervolino A, et al. A fate-mapping approach reveals the composite origin of the connecting tubule and alerts on "single-cell"-specific KO model of the distal nephron. *Am. J. Physiol. Renal Physiol*. 2016;311(5):F901–F906. doi:10.1152/ajprenal.00286.2016
25. Chen L, Chou CL, Knepper MA. Targeted single-cell RNA-seq identifies minority cell types of kidney distal nephron. *J. Am. Soc. Nephrol*. 2021;32 (4):886–896. doi:10.1681/ASN.2020101407
26. Rudman-Melnick V. Single-cell sequencing dissects the transcriptional identity of activated fibroblasts and identifies novel persistent distal tubular injury patterns in kidney fibrosis. *Res Sq*. 2023. doi:10.21203/rs.3.rs-2880248/v1
27. Wu Y, Zhao Y, Yang HZ, Wang YJ, Chen Y. HMGB1 regulates ferroptosis through Nrf2 pathway in mesangial cells in response to high glucose. *Biosci. Rep*. 2021;41(2). doi:10.1042/BSR20202924
28. Tsai CF, Chen G-W, Chen Y-C, et al. Regulatory effects of quercetin on M1/M2 macrophage polarization and oxidative/antioxidative balance. *Nutrients*. 2021;14(1):67. doi:10.3390/nu14010067
29. Li J, Wang T, Liu P, et al. Hesperetin ameliorates hepatic oxidative stress and inflammation via the PI3K/AKT-Nrf2-ARE pathway in oleic acid-induced HepG2 cells and a rat model of high-fat diet-induced NAFLD. *Food Funct*. 2021;12(9):3898–3918. doi:10.1039/d0fo02736g
30. Chen X, Xue H, Fang W, et al. Adropin protects against liver injury in nonalcoholic steatohepatitis via the Nrf2 mediated antioxidant capacity. *Redox Biol*. 2019;21:101068. doi:10.1016/j.redox.2018.101068
31. Lu W, Chen Z, Xu H, et al. Decreased ZMIZ1 suppresses melanogenesis in vitiligo by regulating mTOR/AKT/GSK-3beta-mediated glucose uptake. *In Vitro Cell. Dev. Biol. Anim*. 2023. doi:10.1007/s11626-023-00837-4
32. Cao Y. BHLHE40 inhibits ferroptosis in pancreatic cancer cells via upregulating SREBF1. *Adv Sci (Weinh)*. 2023; e2306298. doi:10.1002/ advs.202306298
33. Pang X, Zhang J, He X, et al. SPP1 promotes enzalutamide resistance and epithelial-mesenchymal-transition activation in castration-resistant prostate cancer via PI3K/AKT and ERK1/2 pathways. *Oxid Med Cell Longev*. 2021;2021:5806602. doi:10.1155/2021/5806602
34. Zhao K, Ma Z, Zhang W. Comprehensive analysis to identify SPP1 as a prognostic biomarker in cervical cancer. *Front Genet*. 2021;12:732822. doi:10.3389/fgene.2021.732822
35. Tsai YC. Single-cell transcriptomic profiles in the pathophysiology within the microenvironment of early diabetic kidney disease. *Cell Death Dis*. 2023;14(7):442. doi:10.1038/s41419-023-05947-1
36. Liu T. Novel synergistic mechanism of 11-keto-beta-boswellic acid and Z-Guggulsterone on ischemic stroke revealed by single-cell transcriptomics. *Pharmacol. Res*. 2023;193:106803. doi:10.1016/j.phrs.2023.106803
37. Zhang Y, Zhao Y, Zhang J, et al. Quantitative proteomics reveals neuroprotective mechanism of ginkgolide b in abeta(1–42)-induced n2a neuroblastoma cells. *J. Integr. Neurosci*. 2023;22(33):33. doi:10.31083/j.jin2202033
38. Kong W, Fu J, Liu N, et al. Nrf2 deficiency promotes the progression from acute tubular damage to chronic renal fibrosis following unilateral ureteral obstruction. *Nephrol. Dial. Transplant*. 2018;33(5):771–783. doi:10.1093/ndt/gfx299
39. Park EJ, Dusabimana T, Je J, et al. Honokiol protects the kidney from renal ischemia and reperfusion injury by upregulating the glutathione biosynthetic enzymes. *Biomedicines*. 2020;8(9):352. doi:10.3390/biomedicines8090352
40. Zhang C, Li H, Qin L, et al. Nuclear receptor AHR-mediated xenobiotic detoxification pathway involves in atrazine-induced nephrotoxicity in quail (Coturnix C. coturnix). *Environ. Pollut*. 2019;253:889–898. doi:10.1016/j.envpol.2019.07.058